

This work was written as part of one of the author's official duties as an Employee of the United States Government and is therefore a work of the United States Government. In accordance with 17 U.S.C. 105, no copyright protection is available for such works under U.S. Law.

Public Domain Mark 1.0

<https://creativecommons.org/publicdomain/mark/1.0/>

Access to this work was provided by the University of Maryland, Baltimore County (UMBC) ScholarWorks@UMBC digital repository on the Maryland Shared Open Access (MD-SOAR) platform.

Please provide feedback

Please support the ScholarWorks@UMBC repository by emailing scholarworks-group@umbc.edu and telling us what having access to this work means to you and why it's important to you. Thank you.



Decoupling error for the atmospheric correction in ocean color remote sensing algorithms

Peng-Wang Zhai^{a,*}, Yongxiang Hu^b, Charles R. Trepte^b, Patricia L. Lucker^a, Damien B. Josset^c

^a SSAI, 1 Enterprise Parkway Suite 200, Hampton, VA 23666, USA

^b MS 475 NASA Langley Research Center, Hampton, VA 23681-2199, USA

^c NASA Postdoctoral Program Fellow, NASA Langley Research Center, USA

ARTICLE INFO

Article history:

Received 8 January 2010

Received in revised form

12 March 2010

Accepted 30 March 2010

Keywords:

Atmospheric and ocean optics

Propagation

Transmission

Attenuation

Radiative transfer

Scattering

Polarization

ABSTRACT

This paper studies the decoupling error associated with the atmospheric correction procedures in the ocean color remote sensing algorithms. The decoupling error is caused by the lack of proper consideration of multiple scattering between the atmospheric and ocean components. In other words, the atmosphere and ocean are not coupled properly. A vector radiative transfer model for the coupled atmosphere and ocean (CAO) system based on the successive order of scattering (SOS) method is used to study the error. The inherent optical properties (IOPs) of the ocean are provided by the most updated bio-optical models. Two wavelengths are used in the study, 412 and 555 nm. For a detector located just above the ocean interface, the decoupling errors range from 0.3% to 7% at 412 nm; and from 0.3% to 3% at 555 nm for zenith viewing angles smaller than 70°. The decoupling errors are significantly larger for larger zenith viewing angles for this detector. For a detector at the top of the atmosphere (TOA), it is hard to separate the decoupling error from the error introduced by the diffuse transmittance. If we assume the upwelling radiance is uniform just below the ocean surface when estimating the diffuse transmittance, the decoupling errors are from −4% to 8% for zenith viewing angles smaller than 70°; and negative decoupling errors show up at mainly large zenith viewing angles.

© 2010 Elsevier Ltd. All rights reserved.

1. Introduction

Ocean color remote sensing is based on the water leaving radiance. In the traditional ocean color retrieval algorithms, water leaving radiance is derived from the total radiance at the top of the atmosphere (TOA) by subtracting the radiance contributions of both the atmosphere and the reflection of the air–sea interface. This is called the atmospheric correction procedure [1–3]. The resultant water leaving radiance is then related to chlorophyll *a* concentration based on semi-empirical relations [4,5]. The water leaving radiance contributes only a small fraction of the total

radiance at the TOA (10% or less). Therefore a small error in the atmospheric correction can lead to a large uncertainty in the retrieved ocean water properties. As an attempt to improve the current ocean color retrieval scheme, another method is to treat the retrieval as an one-step process. This method is a classical inverse problem which involves minimizing of a cost function by comparing the measured radiances with simulated values using a forward radiative transfer model [6,7]. The radiative transfer model used for this purpose in [6,7] is the coupled atmosphere–ocean–discrete ordinate radiative transfer model (CAO-DISORT) [8].

The atmosphere correction procedure normally assumes that the ocean and atmosphere are decoupled, i.e., photons transmitted into the air–sea interface will not be reflected back. Hereafter, this assumption will be called the decoupling approximation. The decoupling

* Corresponding author. Tel.: +1 757 951 1950.

E-mail address: pengwang.zhai-1@nasa.gov (P.-W. Zhai).

approximation has a subtle difference with the black pixel approximation, which assumes the water leaving radiance is zero only at near infrared wavelengths [9]. To date, the error associated with the decoupling approximation has not been quantified yet. The motivation of this paper is to study the percentage error induced by this decoupling approximation in terms of a realistic coupled atmosphere and ocean (CAO) system, which is referred to the decoupling radiance error hereafter. In the following we briefly outline the procedure to define the decoupling error.

For simplicity, we define the atmosphere as a conservative Rayleigh medium with an optical depth of τ_r . The inherent optical properties (IOPs) of the ocean will be derived from a bio-optical model (see Eqs. (62–80) in Ref. [10]). A detector is located in the atmosphere. The optical thickness between the detector and ocean interface is τ_d . In this study we assume the ocean interface is flat. The total radiance $L_{det,total}$ measured by the detector is [1,11]

$$L_{det,total} = L_{det,other} + tL_{wlr}, \quad (1)$$

where the subscript *det* denotes the position of the detector; *t* is the diffuse transmittance; and L_{wlr} is the water leaving radiance just above the ocean surface. Note that the diffuse transmittance is a function of τ_r , τ_d , the water leaving radiance distribution, and the viewing angles [12]. To find $L_{det,other}$, the decoupling schemes assume the atmosphere is bounded by an ocean interface. The ocean is totally absorptive, i.e., the ocean single scattering albedo $\omega_o = 0$. In this decoupled system, the water leaving radiance is simply zero. Then we have the following:

$$L_{det,other} \approx L_{det,total,\omega_o=0}. \quad (2)$$

This equation can be combined with Eq. (1) to solve the water leaving radiance $L_{wlr,dcp}$ in the decoupling approximation. Indeed, the exact values of L_{wlr} , $L_{det,total}$, $L_{det,total,\omega_o=0}$ can be produced by an exact polarized radiative transfer model [10,13]. Thus we can define the decoupling error as

$$\begin{aligned} \eta_{det} &= \frac{L_{wlr,dcp} - L_{wlr}}{L_{wlr}} * 100\% \\ &= \left(\frac{L_{det,total} - L_{det,total,\omega_o=0}}{tL_{wlr}} - 1 \right) * 100\%. \end{aligned} \quad (3)$$

It is then obvious that η_{det} depends on an accurate estimate of the diffuse transmittance. One special case is that the detector is located just above the ocean interface, in which $t=1$. In this case η_{det} measures purely the decoupling error associated with the multiple scattering effects between the atmosphere and ocean. We use 0+ to replace *det* in this case

$$\eta_{0+} = \left(\frac{L_{0+,total} - L_{0+,total,\omega_o=0}}{L_{wlr}} - 1 \right) * 100\%. \quad (4)$$

Another special case is that the detector is located at the TOA, which corresponds to the satellite sensor. In this case, we estimate the diffuse transmittance using the exact radiative transfer model. The system is configured such that the atmosphere is bounded by a flat ocean interface. There is no ocean medium. A light source is

placed just below the ocean interface with uniform upwelling radiance distribution. Two detectors are used to record the radiance distribution in the system; one is located at the TOA and the other just above the ocean interface. After the radiative transfer simulation, we use the following equation to calculate the diffuse transmittance:

$$t^*(\theta, \phi) = \frac{L_{TOA}^*(\theta, \phi)}{L_{0+}^*(\theta, \phi)}, \quad (5)$$

where L_{TOA}^* and L_{0+}^* are the radiances at the TOA and just above the surface for this case, respectively; and θ and ϕ are the zenith and azimuthal viewing angles, respectively. The system configuration and assumptions used here are the same as those of the current MODIS algorithm (see [14, Sec. 3.1.1.5]), though the MODIS algorithm uses the reciprocal method developed in [12]. Note that Eq. (5) is the definition of diffuse transmittance, if the upwelling light source is the same as the true radiance distribution just below the interface. This means that our procedure of estimating the diffuse transmittance is equivalent to the one in the current MODIS algorithm with less theoretical derivations.

Finally, the decoupling error for a detector at the TOA is

$$\eta_{TOA} = \left(\frac{L_{TOA,total} - L_{TOA,total,\omega_o=0}}{t^*L_{wlr}} - 1 \right) * 100\%. \quad (6)$$

It is understood that η_{TOA} measures the total effects of decoupling and the approximation used in the diffuse transmittance calculation, i.e., the uniform radiance distribution just below the ocean surface.

This paper is organized in the following way. Section 2 describes the atmospheric and oceanic optical model and presents the simulation results and discussions. Section 3 is the conclusion.

2. Model and results

The polarized radiative transfer model for a CAO system used in this study is based on the successive order of scattering (SOS) method [10,13]. This SOS model can also generate the water leaving radiance without involving the atmospheric correction procedure. The CAO system is configured in the following way. The atmosphere is taken as a conservative Rayleigh medium. The optical depth of the atmosphere is from Tomasi et al. [15]. No aerosol is included in the atmosphere. The ocean surface is assumed to be flat, i.e., the wind speed is zero. The ocean water is assumed to be Case 1 water [16]. The ocean contains three components, which are pure seawater, phytoplankton pigments, and colored dissolved organic matter (CDOM). The inorganic suspended material is not considered because of their insignificant concentration in Case 1 waters. The IOPs of the ocean include the spectral absorption, scattering, and extinction coefficients, and the scattering Mueller matrix. The total IOPs of the ocean water are modeled as the summation of the contributions of the three components. The bio-optical models for each component are those in Refs. [4,5,17–26].

We refer readers to Eqs. (62–80) in Ref. [10] for explicit formulas and explanations.

Two wavelengths, $\lambda = 412$ and 555 nm, are selected for simulations. The chlorophyll *a* concentrations used are $[\text{Chl}] = 0.3$ and 3 mg m^{-3} . A number of important IOPs of the ocean water are reported in Table 1. The unit of $[\text{Chl}]$ (mg m^{-3}) is omitted in Table 1 for conciseness. The symbols a_t and b_t are the total absorption and scattering coefficients, respectively; b_{bt} is the total backscattering coefficients; B_{bt} is the total backscattering fraction for the ocean water (phytoplankton particles plus the pure sea water); and ω_o is the single scattering albedo. Another important parameter which is not shown in Table 1 is B_{bph} , a dimensionless number which stands for the backscattering fraction of the phytoplankton and covariant particles; in this study B_{bph} is independent of the wavelength [26]. The values of B_{bph} for $[\text{Chl}] = 0.3$ and 3 mg m^{-3} are $8.31\text{E}-3$ and $5.81\text{E}-3$, respectively. The optical depths of the Rayleigh atmosphere are $\tau_r = 0.3186$ and 0.09375 at $\lambda = 412$ and 555 nm, respectively. The ocean optical depth is 10 for both wavelengths. The ocean bottom is set to be totally absorptive. Two solar zenith angles are selected for simulation, $\theta_s = 0^\circ$ and 60° .

Fig. 1 shows η_{0+} for $[\text{Chl}] = 0.3 \text{ mg m}^{-3}$ as a function of viewing angles. The error in this paper is plotted in a polar coordinate system. The center of each circular plate corresponds to the zenith viewing angle $\theta_v = 0^\circ$, while the rim of the plot corresponds to the zenith viewing angle $\theta_v = 70^\circ$. The azimuthal viewing angle ϕ_v of each pixel, as labeled from 0 to 330° in the figure, is equal to the angle formed by the *x*-axis (center to right horizontal line) and the line which connects the pixel to the center.

Fig. 1 shows that η_{0+} is mostly smaller than 1% for the zenith viewing angles smaller than 50° , which agrees the physical intuition that the decoupling error should be small because of small reflectance of typical ocean waters. However, η_{0+} increases as the zenith viewing angle increases. The decoupling error η_{0+} is as large as 6–7% at 412 nm and 2–3% at 555 nm around the zenith viewing of 70° . The error is even larger for the zenith viewing angle larger than 70° , which is not shown in the figure for better clearance at smaller zenith viewing angles. This indicates that measurements for the zenith viewing angle larger than 50° should be used with caution if decoupling scheme is used to derive the water leaving radiance.

Fig. 1 also shows that the error at 412 nm is generally larger than the error at 555 nm. There are two possible explanations for these phenomena. One is the difference of the atmosphere optical depths between the two wavelengths; and the other is the difference of the ocean water IOPs. The atmospheric optical depth affects the

diffuse light illumination just above the ocean surface; and the ocean water IOPs impact the reflectance property. To determine the effects of the ocean water IOP changes, we have calculated η_{0+} at 412 nm by replacing the ocean water IOPs with those at 555 nm. The results show that the changes in η_{0+} are negligible compared to the differences shown in Fig. 1 between the two wavelengths. This practice excludes the differences in the ocean IOPs as a major reason for the differences in η_{0+} at the two wavelengths. The next possible reason is the atmospheric differences. Chowdhary et al. have shown that the water leaving radiance originated from the atmospheric diffuse light is comparable with that from the direct solar light in the blue (410 nm) around solar or viewing zenith angles of 60° . Also the diffuse light contribution increases as the solar/viewing zenith angles increase while the solar direct light contribution shows the opposite trend. Moreover, the diffuse light contribution to the water leaving radiance is less important than the direct light contribution in the green (550 nm). And the diffuse light contribution is less sensitive to the ocean water IOPs [27]. Recall that η_{0+} increases as viewing zenith angle increases, we may draw the conclusion that η_{0+} is mainly caused by the atmospheric diffuse light.

Two additional points are worthy noting in Fig. 1. One is that the decoupling radiance error pattern exhibits little azimuthal dependence even for $\theta_s = 60^\circ$. This is because the decoupling error is related to multiply scattering process, which is largely azimuthally independent. The other is that all the decoupling error shown in Fig. 1 is positive. The reason is that $L_{wlr, dcp}$ overestimates the true water leaving radiance by ignoring all the multiple scattering contributions to $L_{det, other}$.

Fig. 2 shows η_{0+} in the solar principle plane, i.e., the plane contains the solar incident light. This figure is intent to show more numerical details of η_{0+} beyond the color pattern shown in Fig. 1. Negative viewing zenith angles are for the azimuthal angle of $\phi = 180^\circ$, the backscattering half plane, while the positive viewing zenith angles are for $\phi = 0^\circ$, the half plane containing the solar glint. Fig. 2 shows that the differences of η_{0+} at the two $[\text{Chl}]$ values are negligible compared with the effects of the different wavelengths. The reason is the same as that used to explain the differences of η_{0+} at two wavelengths in Fig. 1: the decoupling errors are mainly caused by the atmospheric diffuse light and they are insensitive to the ocean water IOPs.

It is important to understand how the decoupling error affects the satellite remote sensing of ocean color. In this scenario, we need to consider η_{TOA} instead. Fig. 3 shows the decoupling error at the TOA at 412 nm and for the solar zenith angle of $\theta_s = 60^\circ$; and Fig. 4 shows only these errors in the principle plane. Note that the evaluation of the diffuse transmittance assumes the upwelling radiance distribution is uniform just below the ocean surface, which is generally not true. Thus Fig. 3 shows a combined error of the decoupling effects and the diffuse transmittance. Remarkably the decoupling error is between -4% and 4% in this case for zenith viewing angles smaller than 60° . For larger zenith viewing angles, the errors show rather complex pattern. Note that η_{0+}

Table 1
IOPs of Case 1 water.

λ (nm)	$[\text{Chl}]$	a_t (m^{-1})	b_t (m^{-1})	b_{bt} (m^{-1})	B_{bt}	ω_o
412	0.3	3.43E-2	1.74E-1	4.75E-3	2.73E-2	8.35E-1
412	3	1.38E-1	8.12E-1	8.04E-3	9.90E-3	8.55E-1
555	0.3	6.48E-2	1.50E-1	2.16E-3	1.44E-2	6.98E-1
555	3	9.15E-2	8.07E-1	5.60E-3	6.94E-3	8.98E-1

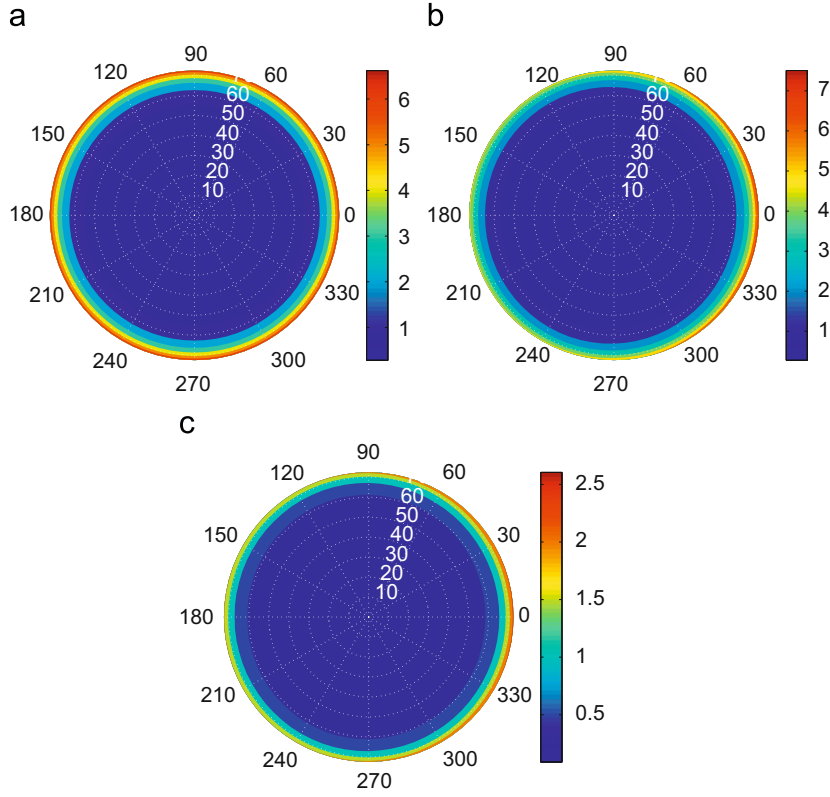


Fig. 1. The decoupling radiance error η_{0+} for $[\text{Chl}] = 0.3 \text{ mgm}^{-3}$. (a) $\theta_s = 0^\circ$ and the wavelength is 412 nm. (b) $\theta_s = 60^\circ$ and the wavelength is 412 nm. (c) $\theta_s = 60^\circ$ and the wavelength is 555 nm.

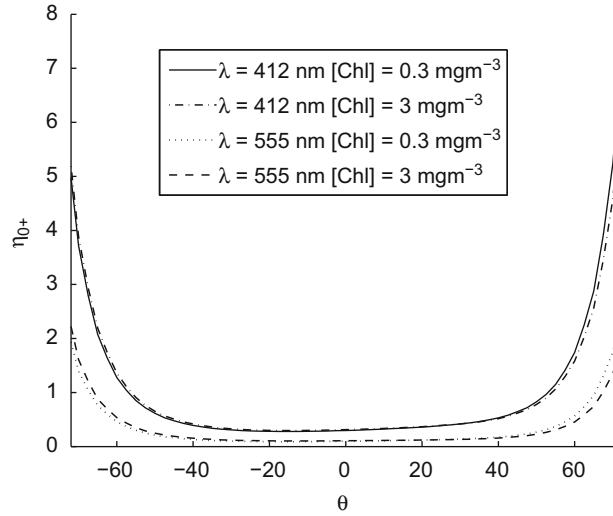


Fig. 2. The decoupling radiance error η_{0+} in the solar principle plane, $\theta_s = 60^\circ$.

should be always positive. This is not the case for η_{TOA} . The error in the diffuse transmittance could lead to negative η_{TOA} values [12], which is observed in many places in Fig. 3 and 4.

The angular patterns of η_{0+} and η_{TOA} are largely different. The error η_{0+} is smooth for most of the cases at

the zenith viewing angles smaller than 40° , while η_{TOA} shows variant patterns for each case. Also η_{TOA} at 412 nm is not always larger than that at 555 nm depending on the viewing angles. This is mainly due to the error in the diffuse transmittance, which is generally 4–6% based on the study by Yang and Gordon [12].

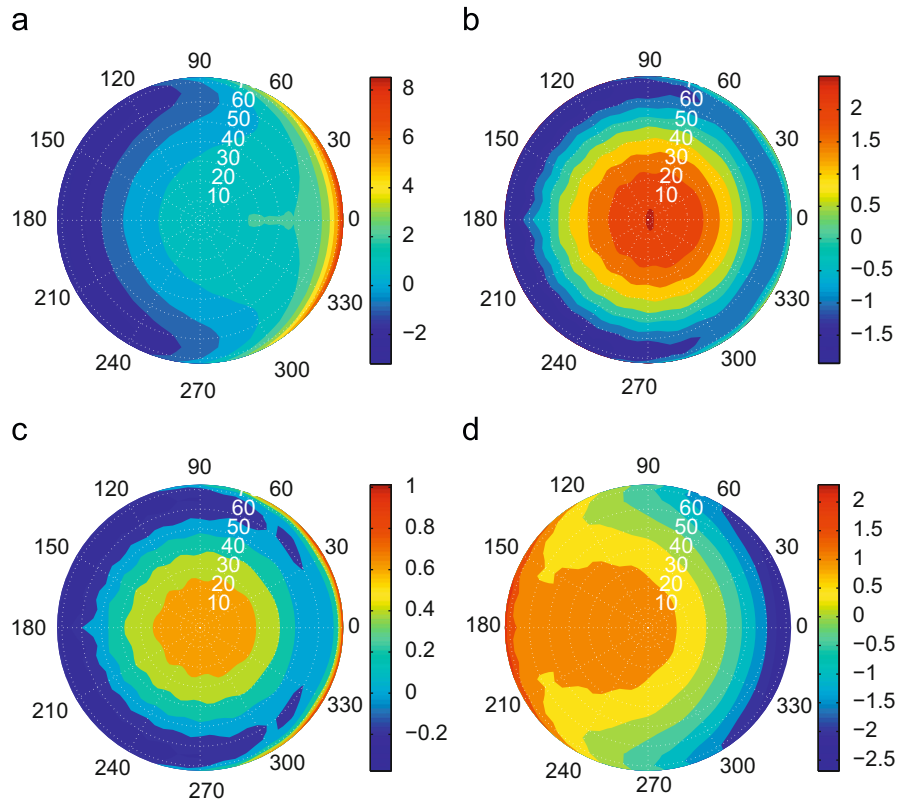


Fig. 3. The decoupling radiance error η_{TOA} , $\theta_s = 60^\circ$. (a) The chlorophyll a concentration is $[Chl] = 0.3 \text{ mg m}^{-3}$ and the wavelength is 412 nm. (b) The chlorophyll a concentration is $[Chl] = 3 \text{ mg m}^{-3}$ and the wavelength is 412 nm. (c) The chlorophyll a concentration is $[Chl] = 3 \text{ mg m}^{-3}$ and the wavelength is 555 nm. (d) The chlorophyll a concentration is $[Chl] = 3 \text{ mg m}^{-3}$ and the wavelength is 555 nm.

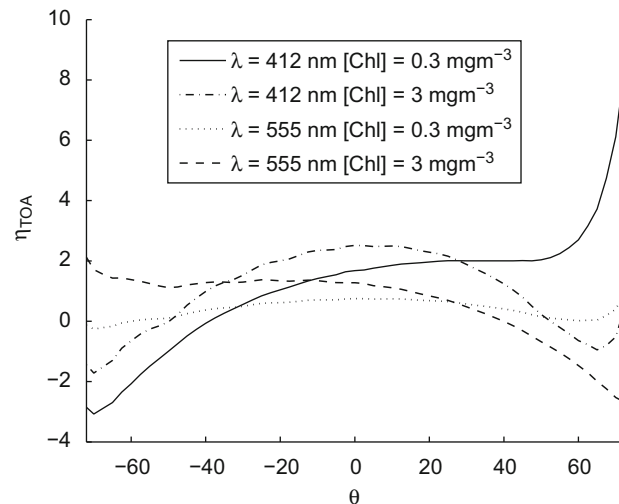


Fig. 4. The decoupling radiance error η_{TOA} in the solar principle plane, $\theta_s = 60^\circ$.

3. Conclusion

This paper studies the decoupling error related to the atmospheric correction for ocean color remote sensing. For a detector located just above the ocean interface, the decoupling scheme generally overestimates the water

leaving radiance from 0.3% to 1% for zenith viewing angles smaller than 50° . It is significantly larger (up to 7% around $\theta_v = 70^\circ$), however, for larger viewing angles. This error is larger at 412 nm than the error at 555 nm. Simulations have also shown that this error is insensitive to the solar zenith angle and chlorophyll a concentration. For a

detector at the TOA, the error is generally within 4% and shows much larger variances with the viewing angles due to error contributions from the approximation used for the diffuse transmittance. It should be noted that the empirical algorithms use the water leaving radiance ratios to derive chlorophyll *a* concentration [11], which means that the error in chlorophyll *a* concentration due to the decoupling error may be limited.

Acknowledgements

This study is supported by the NASA Radiation Science program administrated Hal Maring and the Biogeochemistry program administrated by Paula Bontempi. We would like to thank A. Bricaud for the absorption coefficient data. We also gratefully acknowledge the two anonymous reviewers for their comments about the diffuse transmittance calculation and origin of the decoupling error.

References

- [1] Gordon HR, Wang M. Retrieval of water-leaving radiance and aerosol optical thickness over the oceans with SeaWiFS: a preliminary algorithm. *Appl Opt* 1994;33:443–52.
- [2] Wang M, Gordon HR. A simple moderately accurate atmospheric correction algorithm for SeaWiFS. *Remote Sens Environ* 1994;50:231–9.
- [3] Gordon HR. Atmospheric correction of ocean color imagery in the Earth observing system era. *J Geophys Res* 1997;102:17081–106.
- [4] Loisel H, Morel A. Light scattering and chlorophyll concentration in case 1 waters: a reexamination. *Limnol Oceanogr* 1998;43:847–58.
- [5] Morel A, Maritorena S. Bio-optical properties of oceanic waters: a reappraisal. *J Geophys Res* 2001;106:7163–80.
- [6] Stamnes K, Li W, Yan B, Eide H, Barnard A, Pegau WS, et al. Accurate and self-consistent ocean color algorithm: simultaneous retrieval of aerosol optical properties and chlorophyll concentrations. *Appl Opt* 2003;42:939–51.
- [7] Spurr R, Stamnes K, Eide H, Li W, Zhang K, Stamnes JJ. Simultaneous retrieval of aerosols and ocean properties: a classic inverse modeling approach. I. Analytic Jacobians from the linearized CAODISORT model. *J Quant Spectrosc Radiat Transfer* 2007;104:428–49.
- [8] Jin Z, Charlock TP, Rutledge K, Stamnes K, Wang Y. Analytical solution of radiative transfer in the coupled atmosphere–ocean system with a rough surface. *Appl Opt* 2006;45:7443–55.
- [9] Siegel DA, Wang M, Maritorena S, Robinson R. Atmospheric correction of satellite ocean color imagery: the black pixel assumption. *Appl Opt* 2000;39:3582–91.
- [10] Zhai P, Hu Y, Chowdhary J, Trepte CR, Lucker PL, Josset DB. A vector radiative transfer model for coupled atmosphere and ocean systems with a rough interface. *J Quant Spectrosc Radiat* 2010;111:1025–40 <<http://www.sciencedirect.com/science/article/B6TVR-4Y05DRB-2/2/4b85aa253ecf832e93f2eac40e17c0e4>>.
- [11] Gordon HR, Clark DK, Brown JW, Brown OB, Evans RH, Broenkow WW. Phytoplankton pigment concentrations in the Middle Atlantic Bight: comparison of ship determinations and CZCS estimates. *Appl Opt* 1983;22:20–36.
- [12] Yang H, Gordon HR. Remote sensing of ocean color: assessment of water-leaving radiance bidirectional effects on atmospheric diffuse transmittance. *Appl Opt* 1997;36:7887–97 <<http://www.opticsinfobase.org/ao/abstract.cfm?URI=ao-36-30-7887>>.
- [13] Zhai P, Hu Y, Trepte CR, Lucker PL. A vector radiative transfer model for coupled atmosphere and ocean systems based on successive order of scattering method. *Opt Express* 2009;17:2057–79.
- [14] Gordon HR, Voss KJ. MODIS normalized water-leaving radiance, Version 5, Algorithm Theoretical Basis Document (MOD 18). 2004; <http://modis.gsfc.nasa.gov/data/atbd/atbd_mod18.pdf>.
- [15] Tomasi C, Vitale V, Petkov B, Lupi A, Cacciari A. Improved algorithm for calculations of Rayleigh-scattering optical depth in standard atmospheres. *Appl Opt* 2005;44:3320–41.
- [16] Morel A, Prieur L. Analysis of variations in ocean color. *Limnol Oceanogr* 1977;22:709–22.
- [17] Pope RM, Fry ES. Absorption spectrum (380–700nm) of pure water. II. Integrating measurements. *Appl Opt* 1997;33:8710–23.
- [18] Bricaud A, Morel A, Prieur L. Absorption by dissolved organic matter of the sea (yellow substance) in the UV and visible domains. *Limnol Oceanogr* 1981;26:43–53.
- [19] Bricaud A, Morel A, Babin M, Allali K, Claustre H. Variations of light absorption by suspended particles with chlorophyll *a* concentration in oceanic (case 1) waters: analysis and implications for bio-optical models. *J Geophys Res* 1998;103:31033–44.
- [20] Mobley CD. Light and water: radiative transfer in natural waters. San Diego: Academic; 1994.
- [21] Fourier G, Forand JL. Analytic phase function for ocean water. In: Jaffe JS, editor. *Ocean optics XII. Proc SPIE*, vol. 2258; 1994. p. 194–201.
- [22] Fournier G, Jonasz M. Computer-based underwater imaging analysis. In: Gilbert G, editor. *Airborne and in-water underwater imaging. Proc SPIE*, vol. 3761; 1999. p. 62–77.
- [23] Mobley CD, Sundman LK, Boss E. Phase function effects on oceanic light fields. *Appl Opt* 2002;41:1035–50.
- [24] Petzold TJ. Volume scattering functions for selected ocean waters. Scripps Institution of Oceanography; 1977.
- [25] Voss KJ, Fry ES. Measurement of the Mueller matrix for ocean water. *Appl Opt* 1984;23:4427–39.
- [26] Huot Y, Morel A, Twardowski MS, Stramski D, Reynolds RA. Particle optical backscattering along a chlorophyll gradient in the upper layer of the eastern South Pacific Ocean. *Biogeosciences* 2008;5:495–507.
- [27] Chowdhary J, Cairns B, Travis LD. Contribution of water-leaving radiances to multiangle, multispectral polarimetric observations over the open ocean: bio-optical model results for case 1 waters. *Appl Opt* 2006;45:5542–67 <<http://www.opticsinfobase.org/abstract.cfm?URI=ao-45-22-5542>>.